Beam and phase distributions of a terahertz quantum cascade wire laser

M. Cui,[1,2,a)] J. N. Hovenier,[2] Y. Ren,[2,3] N. Vercruyssen,[1,2] J. R. Gao,[1,2,a)] T. Y. Kao,[4] Q. Hu,[4] and J. L. Reno[5]
[1]*SRON Netherlands Institute for Space Research, Sorbonnelaan 2, 3584 CA Utrecht, The Netherlands*
[2]*Kavli Institute of Nanoscience, Delft University of Technology, Lorentzweg 1, 2628 CJ, Delft, The Netherlands*
[3]*Purple Mountain Observatory (PMO), Chinese Academy of Science, 2 West Beijing Road, Nanjing, JiangSu 210008 and Graduate School, Chinese Academy of Sciences, 19A Yu Quan Road, Beijing 100049, China*
[4]*Department of Electrical Engineering and Computer Science, Massachusetts Institute of Technology, Cambridge, Massachusetts 02139, USA*
[5]*Center for Integrated Nanotechnologies, Sandia National Laboratories, Albuquerque, New Mexico 87185-0601, USA*

(Received 5 January 2013; accepted 12 March 2013; published online 22 March 2013)

We report on both measurements and simulations of the beam profile and wavefront of a single-mode, 3.5 THz quantum cascade wire laser, incorporating a lateral corrugated metal-metal waveguide, 3rd-order distributed feedback grating. The intrinsic wavefront was measured by using a Hartmann wavefront sensor (HWS) without any optical components between the laser and HWS. Both beam profile and wavefront were simulated using an antenna array model, but taking the non-uniform electric field distribution along the waveguide into account. The results show that the non-uniform distribution along the wire laser plays a crucial role in realizing a nearly single-lobed narrow beam. The measured wavefront is spherical and agrees well with the simulation. © *2013 American Institute of Physics*. [http://dx.doi.org/10.1063/1.4798250]

Quantum cascade wire lasers (QCWLs)[1–3] incorporating a lateral corrugated metal-metal waveguide, 3rd-order distributed feedback (DFB) grating are attractive for applications because of their high-temperature operation, low operating power, controllable single-mode emission, mW output power, and single-lobed low divergent beam. In particular, the high-temperature operation and low operating power take advantage of the low-loss double metal waveguide wire laser with a sub-wavelength transverse dimension. The robust single-mode emission is extracted efficiently from the active region of GaAs/AlGaAs by a 3rd-order Bragg grating. Promising 3rd-order DFB QCWLs that deliver single-mode output power of more than 1.5 mW have been demonstrated at 3.5 THz. These QCWLs can be operated in CW mode up to 110 K, but consume less than 300 mW DC power.[2] 3rd-order DFB QCWLs have further been demonstrated as local oscillators in heterodyne spectrometers centered at 3.5 THz and 4.7 THz, respectively.[4,5]

To overcome the diffraction limit of THz sub-wavelength wire lasers, an antenna model has been proposed and a narrow far-field beam was predicted if the longitudinal phase velocity within the laser matches the one in the free-space.[6] However, it is only recently that such a beam has been realized for THz QCWLs by using a 3rd-order lateral corrugated grating,[2] which is equivalent to a periodic array of apertures along the waveguide with a periodicity of roughly half of the free-space wavelength λ_0. One can then apply an end-fire antenna array model. The narrow beam was a result of the radiation added constructively from all the apertures. Interestingly, the observed narrow, single-lobed beams were apparently better than model calculations. The latter show the clear presence of side lobes. Another approach to realize a low divergent beam is to have a similar 3rd-order DFB grating, but adding additional contact fins to achieve the perfect phase-match. The perfect phase matching allows many more periods (~151 periods) that resulted in a narrow main beam.[3]

It is known that both intensity and phase distributions of a beam are crucial for optimizing its propagation and beam matching in an optical system. The beam intensity profile has been recognized as one of the important performances for THz quantum cascade lasers (QCLs), reflected by many literatures on this topic. The importance of the phase was also demonstrated in an experiment where a QCL was used as a local oscillator to pump an antenna coupled, coherent superconducting detector.[7] However, the phase of the QCL beam has never been directly measured. The wavefronts, containing the phase information, have recently been studied using the Hartmann wavefront sensor (HWS) for a beam generated by a few designed phase objects using a Far Infrared (FIR) gas laser as the THz source[8] and for a beam generated by two focused lenses using a QCL as the source.[9] Until now, the intrinsic wavefront of a 3rd-order DFB QCWL has never been reported.

In this paper, we measured both beam intensity and wavefront of a 3.5 THz QCWL based on a 3rd-order DFB grating. They are intrinsic to the laser because no optical components are placed in front of the laser. We also performed calculations for both beam intensity and wavefront using a model similar to an end-fire antenna array, but taking the non-uniform electric field distribution along the laser into account and compared with the measurement results.

The working principle of a 3rd-order DFB QCWL is illustrated in Fig. 1(a), where the 3rd-order diffracted optical

a)Authors to whom correspondence should be addressed. Electronic addresses: m.cui@vu.nl and j.r.gao@tudelft.nl

mode is used for the distributed feedback and the 1st and 2nd-order diffracted modes for the out-coupling. The active region of the QCWL is made of GaAs/AlGaAs, with a refractive index of ~3.6, imbedded within double metal layers, which together form a waveguide structure. The Bragg reflector is formed by a grating of slits. The periodic array of opening slits can extract single-mode frequency radiation from the active medium; while the periodicity designed to be roughly half of the free space wavelength allows the radiation from all slits adding up constructively along the direction of waveguide. The DFB grating hence forms a concentrated narrow beam in a similar way as a one-dimensional end-fire antenna array. The effective refractive index n_{eff} is defined as $n_{eff} = 3\lambda_0/(2\Lambda)$, where Λ is the grating period. When $n_{eff} = 3$, both the 1st and 2nd-order diffracted modes can be coupled out and propagate along the top surface of the waveguide because they can match the wave vector of the mode propagating in air in this direction.[1] So, the laser can perfectly meet the requirement of edge emitting through the slits. However, taking the finite length of the QCWL into account, the light can also be coupled out of the laser even when n_{eff} is slightly larger than 3. This is because when the grating has a finite number of periods, the diffraction angle caused by the Bragg reflector is not a single value, but with a certain range.[10]

The laser used for both beam pattern and wavefront measurements is a 3rd-order DFB structure, which emitted a single-mode at 3.45 THz. The 10-μm thick active region is based on a four-well resonant-phonon depopulation design.[11] The wire laser incorporates a metal-metal waveguide and has a cavity structure with a lateral corrugated grating of square teeth. It has a waveguide ridge width of 50 μm, 27 periods with a Λ of 39.63 μm, and a slit opening of 5.84 μm. The effective refractive index corresponds to ~3.2. When operated with 3 W DC input power and at a temperature of ~12 K, the laser provides a maximum output power of roughly 0.8 mW.

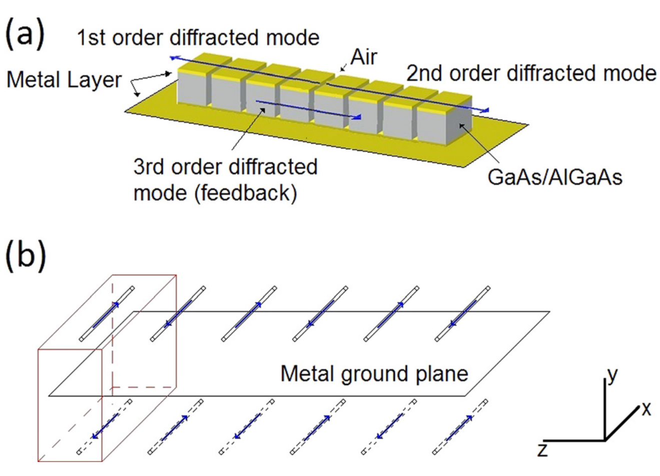

FIG. 1. (a) Schematic of a THz quantum cascade wire laser based on 3rd-order distributed feedback grating. The active region of the laser is made of GaAs/AlGaAs. The layers in yellow on both top and bottom of the laser are metal layers. The Bragg reflector is introduced by the deep air slits. Three different diffracted modes are explained in the text. (b). Schematic depicts an effective dipole model using the slot-dipole duality based on Babinet's principle (see Ref. 13). The effect of the metal ground plane can be taken into account by using the method of image. The coordinate used in the simulation is illustrated at the right-down corner.

For the beam pattern and wavefront measurements, no lenses or other optical components were placed in front of the laser except for an optically thin window made out of 2 mm thick high-density polyethylene. The laser was operated in a pulse tube cooler with a temperature of ~12 K and was biased in a pulsed mode with an averaged current of 50 mA and a voltage of 1 V above its lasing threshold bias of 150 mA and 13.6 V (corresponding to a threshold current density J_{th} of 310 A/cm^2). The intensity profiles were measured by a pyroelectric detector together with a lock-in amplifier scanned in two dimensions (2D) in an x-y plane at a distance of 30 ± 1 mm away from the center of the QCWL and is normal to the waveguide direction. Fig. 2(a) shows the measured beam intensity within an area of 30 mm × 30 mm in a 2D fashion. The center of the plot (0,0) corresponds to the projected position of the waveguide on the observation plane. A few observed features are worthwhile to mention. Beyond this 30 mm × 30 mm area in the figure, we could not find measurable intensity signal in our case. Therefore, we conclude that it is a nearly single-lobed beam or is at least dominated by the main lobe. The main beam is not symmetrical and deviates considerably from an ideal Gaussian beam. The width of the main beam (full width half maximum) is roughly 7 mm × 9 mm, which correspond to angles of 13° × 17°.

The beam patterns of similar lasers have been calculated in two methods. One is to use a formalism originally used for an end-fire antenna array at microwave frequency, called *the array antenna model*. The openings of the lateral corrugated teeth in the 3rd-order DFB grating are modeled as square apertures, all of which have the same amplitude of the electrical field or equivalently the same dipole current. Therefore, the field distribution within the antenna array in

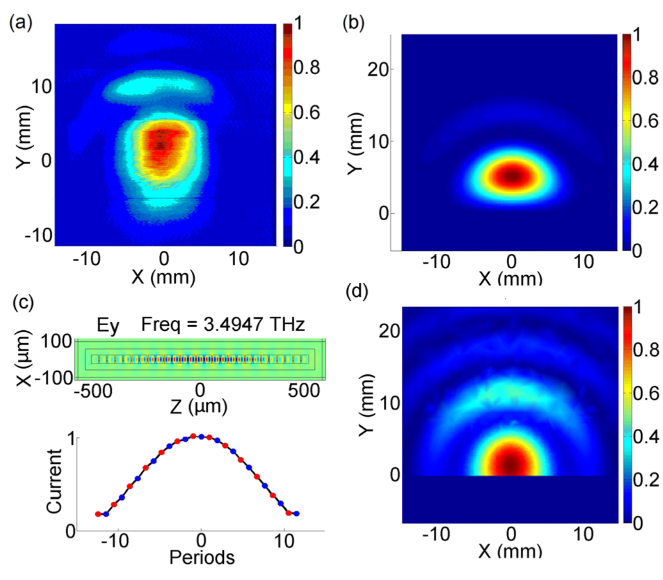

FIG. 2. (a) The measured intensity distribution of the 3.5 THz 3rd-order distributed feedback quantum cascade wire laser. The observation plane is 30 mm in front of the center of the laser. The projected position of the wire laser on the observation plane is (0,0); (b) the simulated intensity pattern of the 3.5 THz wire laser in the same condition as the measurement; (c) the electric field (upper) calculated from the FEM and the current distribution (below) used in the antenna array model. The dipole currents are proportional to the electric field at y = 0; and (d) The Fourier transform of the near field simulated by FEM.

this case was uniform. As shown in Refs. 2 and 10, the calculated beams, especially for the case where $n_{eff} > 3$, have more pronounced side-lobes than what was observed in practice, where the measured beams were nearly single-lobed. The 2nd method is to calculate the electro-magnetic field distribution numerically using a finite element method (FEM) and then to obtain the far-field beam pattern by Fourier transformation.[10] This method allows calculating the electric or magnetic field distribution inside the laser. However, the calculated beam patterns show the effect of the side lobes to be even stronger than what was observed experimentally. The cause is unclear. Here, we take a different approach to model our laser structures by taking the array antenna model and incorporating the electrical field for each antenna calculated by FEM, which is non-uniformly distributed along the waveguide.[12]

An effective dipole model based on the slot-dipole duality according to Babinet's principle[13] is shown schematically in Fig. 1(b). The radiation is emitted from the narrow openings on the top metal layer of the waveguide. Each of the openings can be represented by a dipole whose length equals to the width of the waveguide. The dipole current is proportional to the electrical field on each opening.[14] The emitted electric field of a dipole in the far-field is expressed as[13]

$$E \propto \frac{Ie^{-jkr}}{r}\sqrt{1-\sin^2\theta\sin^2\phi}, \qquad (1)$$

where k is the wave vector and I the dipole current. The transformation from the Cartesian coordinate shown in the inset of Fig. 1(b) to the spherical coordinate is

$$\begin{gathered} r^2 = x^2 + y^2 + z^2 \\ \cos\theta = y/r \quad \tan\phi = x/z. \end{gathered} \qquad (2)$$

The QCWL is considered as an array of one-dimensional dipoles separated by the DFB grating period ($\sim\lambda_0/2$). The phase shift from its neighboring antenna is always 3π.[2,3] The metal ground plane in Fig. 1(b) is considered as an infinite perfect mirror in the calculation, whose effect can be modeled by using the method of images.[15] The far-field in the direction of an end-fire antenna array is then the radiation added coherently for all the dipoles and can be calculated numerically using

$$E_N \propto \sum_{n=1}^{N}\frac{I_n e^{-jkr_n}}{r_n}\sqrt{1-\sin^2\theta_n\sin^2\phi_n}, \qquad (3)$$

where N is the number of opening slits of the QCWL.

Fig. 3 shows our simulated intensity in the far-field with a variation of both the electric field distribution along the wire laser and the effective refractive index. To make a direct comparison with the measurement easier, the simulation was performed for a laser being similar to the measured one (3.5 THz and 27 periods). The beam profiles are calculated for the x-y plane, which is taken 30 mm away from the center of the QCWL by assuming three different n_{eff}, which is 3.0, 3.2, and 3.4, respectively, and several dipole current distributions across the antenna array. The latter are chosen to be a uniform, a triangle, and two Gaussians in order to differentiate their effects. We included n_{eff} of 3.2 and 3.4 because those values are practically found in Refs. 1 and 2. The two Gaussian profiles have a different width defined by σ, which has 6 periods ($\sigma = 6$) and 11 periods ($\sigma = 11$), respectively. When $n_{eff} = 3.0$, all four of the distributions give relatively concentrated beams with very weak side-lobes. However, when n_{eff} is 3.2, the triangle and 1st Gaussian current distributions result in a single- or multi-lobed beam. In this case, the main lobe corresponding to the triangle current distribution contains 67% of the total energy within the plotted beam area, in contrast to a value of 19% corresponding to the uniform current distribution. In the case of $n_{eff} = 3.4$, only the triangle distribution can still result in a concentrated beam, although strongly curved. Our simulation shows that the electric field distribution along the waveguide of the wire laser plays a crucial role in realizing a single-lobed narrow beam. If we use a Gaussian current distribution where σ is reduced to 5 periods, even with a n_{eff} of 3.4, the far-field has no side lobes. As pointed out in Ref. 3, when the phase is not perfectly matched ($n_{eff} \neq 3$), there is a maximum coherence length L_c beyond which the field from different slits will superpose destructively, where $L_c = \Lambda \times n_{eff}/|n_{eff} - 3|$. Clearly, the total output power will actually *decrease* as the length of the ridge increases beyond L_c. The current investigation shows that not only the total power but also the beam pattern will suffer for a mismatched 3rd-order DFB laser. The tapered current profiles along the DFB structure in Fig. 3 effectively shorten the length of the laser, alleviating the detrimental effect of phase mismatching.

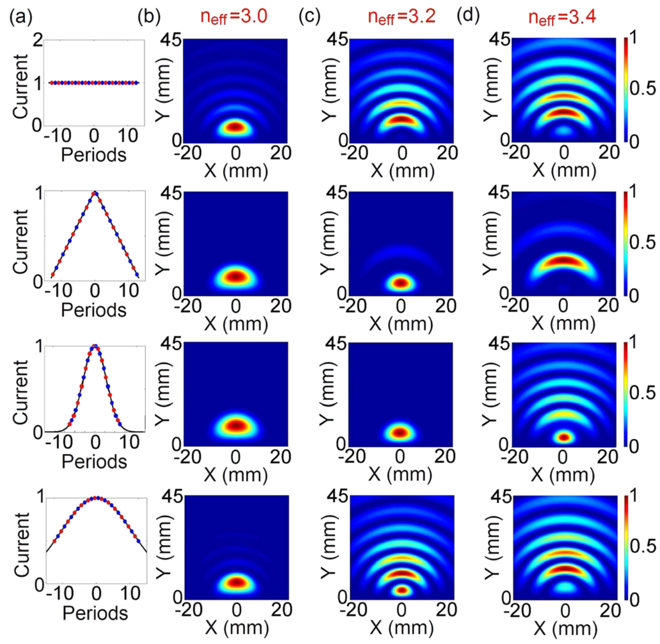

FIG. 3. Simulated far-field intensity distributions at a distance of 30 mm away from the quantum cascade wire laser. The first row: a uniform distribution of dipole currents. From the left to the right, (a) the current distribution inside the laser. The red dots represent dipoles with positive current and the blue dots represent dipoles with negative current. The effective refractive index is (b) 3.0, (c) 3.2, and (d) 3.4, respectively. The second row: a triangle distribution of the dipole currents. The third row: Gaussian distribution of the dipole currents with a width of σ, which equals 6 periods. The fourth row: Gaussian distribution of the dipole currents with $\sigma = 11$ periods.

To compare with the measured beam profile, we calculated the beam using our antenna array model based on the electrical field profile, which was computed by three-dimensional FEM for the lasing mode of 3.4947 THz.[3] The electric field component E_y, which dominates the fields inside the QCWL, is imaged in the top panel of Fig. 2(c). The relative current profile along the wire laser, which is proportion to the local E_y, is plotted in the low panel of Fig. 2(c). The beam pattern is calculated using Eq. (3) based on the same laser parameters as in the experiment and the current profile in Fig. 2(c). The antenna array model does predict an approximately single-lobed beam as observed in the experiment. The main lobe accounts for 86% of the total output energy within the plotted beam area, which agrees with the measured value of 81%. However, there are discrepancies with regard to the beam size and the position of the beam. To complete the comparison, we also include the beam pattern calculated using the FEM in combination with Fourier transformation in Fig. 2(d). We find the beam size is comparable to the one calculated by the array antenna model. But there are relatively strong side lobes as found in Refs. 3 and 10.

The wavefront was studied using a HWS.[8,16] The measurement setup is schematically shown in Fig. 4(a). Our HWS has been carefully designed by combining the spatial resolution with the wavefront sensitivity and well calibrated with a sensitivity of less than 14 mrad and a dynamic range of 0.2 rad.[8] The measured accuracy of the wavefront is better than $0.5\lambda_0$. The Hartmann mask is based on a 0.2 mm thick copper plate whereby the holes in the array are 1 mm in diameter and have 3 mm in periodicity. The Hartmann mask is mounted on a 2D translation stage and is moved 9 times with a 1 mm step in both x and y directions during a wavefront measurement to increase the spatial resolution. The Hartmann mask is located at a distance of 28 ± 1 mm away from the center of the QCWL. We used the pyroelectric detector, mounted on a 2D translation stage, to measure the imaging spot field generated by the Hartmann mask in the detection plane. The distance between the Hartmann mask and the detection plane is 7 mm.

To illustrate a measured wavefront of the wire laser, we start with Fig. 4(b) showing one of the directly recorded imaging spot fields and with Fig. 4(c) that combines the centroids of all the 9 images and summarizes a complete extracted spot field.[8] The wavefront is reconstructed from the extracted spot field by using Zonal wavefront estimation, and the result is shown in Fig. 4(d). This wavefront covers the area of 10×10 mm^2, the center of which roughly overlaps the center in the beam pattern plot in Fig. 2(a). Since the QCWL was not fully located at the center of the spot field coordinate, to obtain a symmetric wavefront, we shift manually the Hartmann mask in order to coincide the hole array with the extracted spot field. This procedure is mathematically equivalent to subtracting the tilt terms in the Zernike polynomials. Before we compare the result with a model prediction, it is important to notice that the measured wavefront has a nearly spherical shape. Based on the averaged spot separation of 1.245 ± 0.008 mm that was derived from Fig. 4(c), we find the radius of spherical wavefront to be 28.6 ± 0.9 mm.[17]

The wavefront of the QCWL beam was also modeled using the non-uniform antenna array model. According to Eq. (1), the electric field of a dipole in the far-field ($\vec{k} \cdot \vec{r} \gg 1$) with the same phase is spherical. Thus, the wavefront is spherical too. For an array antenna, there is an additional phase factor that represents the phase shift of the array's phase centre relative to the origin. However, it is equal to one if the origin coincides with the array's centre. Therefore, the wavefront in the far-field formed by the array of dipoles should be spherical. We simulated the wavefront based on the array antenna and find that in the far-field, it is indeed very spherical. Quantitatively, when the plane for measuring the wavefront is at a distance of more than $100 \times \lambda_0$ away from the center of the QCWL, resulting in the Fresnel number to be $\ll 1$, the calculated wavefront deviates from a perfectly spherical one by less than $0.01 \times \lambda_0$.

Fig. 4(e) shows the simulated wavefront of the QCWL for the plane of the Hartmann mask, which is spherical and has a radius of 28 mm. The latter is confirmed by the measured value of 28.6 ± 0.9 mm. The overall difference between the measured wavefront and simulated one is also calculated and is shown in Fig. 4(f). The maximal deviation between the two is $\pm 0.3\lambda_0$, which is just about the accuracy of our HWS. This deviation could also be due to a misalignment of the Hartmann mask with respect to the x-y detection plane since Fig. 4(f) shows a small tilt with respect to the x-y plane. It is interesting to notice that, in contrast to the far-field intensity pattern that was not a Gaussian, the measured

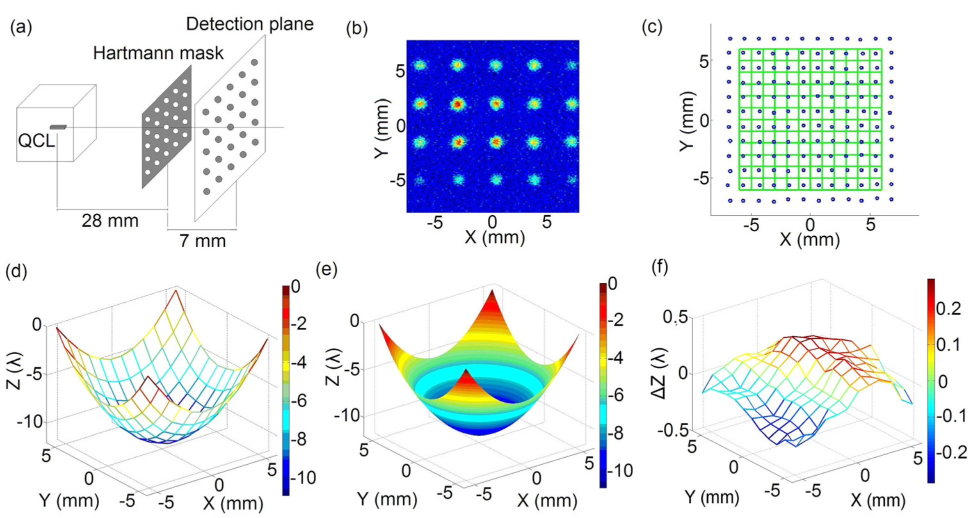

FIG. 4. (a) The HWS setup to measure the wavefront of the laser. The Hartmann mask is located 28 mm away from the center of the wire laser. The observation plane is 7 mm behind the Hartmann mask; (b) directly measured spot field of the incident THz wavefront in the detection plane for a given Hartmann mask position; (c) the HWS spot field that consists of the extracted centroids of the imaging spots in (b), but measured by shifting the Hartmann mask by 1 mm in either x- or y-direction and in total 9 times; (d) the measured wavefront. (e) The simulated wavefront by using the antenna array model; (f) the phase difference between (d) and (e).

wavefront of the QC wire laser has almost an ideal spherical contour. Although not measured, the wavefront in the near field is expected to be non-spherical.

In conclusion, we measured the far-field beam profiles in both intensity and phase for a THz single-mode quantum cascade wire laser. We find that, although not an ideal Gaussian, the intensity profile is narrow, nearly single-lobed and can be explained by the non-uniform electric field distribution antenna array model. The measured wavefront is spherical and agrees with that predicted by the antenna array model. Our work suggests that one can further shape the far-field intensity beam by engineering the electric field distribution along the wire laser.

The authors acknowledge D. J. Hayton, T. M. Klapwijk, H. P. Urbach, and A. Neto for helpful discussions. The work in the Netherlands was supported by NWO, KNAW China Exchange Programme, and NATO SFP. The work at MIT was supported by NASA and NSF. The work at Sandia was performed, in part, at the Center for Integrated Nanotechnologies, a U.S. Department of Energy, Office of Basic Energy Sciences user facility. Sandia National Laboratories is a multi-program laboratory managed and operated by Sandia Corporation, a wholly owned subsidiary of Lockheed Martin Corporation, for the U.S. Department of Energy National Nuclear Security Administration under Contract DE-AC04-94AL85000.

[1]M. I. Amanti, M. Fischer, G. Scalari, M. Beck, and J. Faist, Nat. Photonics **3**, 586 (2009).
[2]M. I. Amanti, G. Scalari, F. Castellano, M. Beck, and J. Faist, Opt. Express **18**, 6390 (2010).
[3]T. Y. Kao, Q. Hu, and J. L. Reno, Opt. Lett. **37**, 2070 (2012).
[4]Y. Ren, J. N. Hovenier, R. Higgins, J. R. Gao, T. M. Klapwijk, S. C. Shi, B. Klein, T. Y. Kao, Q. Hu, and J. L. Reno, Appl. Phys. Lett. **98**, 231109 (2011).
[5]J. L. Kloosterman, D. J. Hayton, Y. Ren, T. Y. Kao, J. N. Hovenier, J. R. Gao, T. M. Klapwijk, Q. Hu, C. K. Walker, and J. L. Reno, Appl. Phys. Lett. **102**, 011123 (2013).
[6]E. E. Orlova, J. N. Hovenier, T. O. Klaassen, I. Kašalynas, A. J. L. Adam, J. R. Gao, T. M. Klapwijk, B. S. Williams, S. Kumar, Q. Hu, and J. L. Reno, Phys. Rev. Lett. **96**, 173904 (2006).
[7]P. Khosropanah, W. Zhang, J. N. Hovenier, J. R. Gao, T. M. Klapwijk, M. I. Amanti, G. Scalari, and J. Faist, J. Appl. Phys. **104**, 113106 (2008).
[8]M. Cui, J. N. Hovenier, Y. Ren, A. Polo, and J. R. Gao, Opt. Express **20**, 14380 (2012).
[9]H. Richter, M. Greiner-Bär, N. Deßmann, J. Pfund, M. Wienold, L. Schrottke, R. Hey, H. T. Grahn, and H. W. Hübers, Appl. Phys. Lett. **101**, 031103 (2012).
[10]M. I. Amanti, "Photonics for THz quantum cascade lasers," Ph.D. dissertation (ETH ZURICH, 2010).
[11]Q. Qin, B. S. Williams, S. Kumar, J. L. Reno, and Q. Hu, Nat. Photonics **3**, 732 (2009).
[12]H. Kogenlnik and C. V. Shank, J. Appl. Phys. **43**, 2327 (1972).
[13]C. A. Balanis, *Antenna Theory: Analysis and Design* (J. Wiley and sons, 2005).
[14]Strictly speaking, we should use a magnetic field instead of the electric field. Our FEM simulation shows that inside the slit, the amplitude of the electric field is always proportional to the magnetic field, while the direction is perpendicular to the magnetic field.
[15]J. D. Jackson, *Classical Electrodynamics* (John Wiley & Sons, 1962).
[16]A review, see B. C. Platt and R. Shack. J. Refract. Surg. **17**, S573 (2001).
[17]The radius of spherical wavefront is given by $L/(x\text{-}p)$, where L ($= 7$ mm) is the distance between the mask and the detection plane, x the measured averaged spot separation, and $p(= l$ mm) the effective hole separation in the mask.